RANS simulations of wind flow at the Bolund experiment

D. Cabezón[1)], J. Sumner[2)], B. Garcia[1)], J. Sanz Rodrigo[1)], C. Masson[2)]

[1)] Department of Wind Energy, National Renewable Energy Centre (CENER), Spain
[2)] Department of Mechanical Engineering, École de Technologie Supérieure (ÉTS), Montreal, Canada

Abstract

As part of their development, the predictions of numerical wind flow models must be compared with measurements in order to estimate the uncertainty related to their use. Of course, the most rigorous such comparison is under blind conditions. The following paper includes a detailed description of three different wind flow models, all based on a Reynolds-averaged Navier-Stokes approach and two-equation k-ε closure, that were tested as part of the Bolund blind comparison (itself based on the Bolund experiment which measured the wind around a small coastal island). The models are evaluated in terms of predicted normalized wind speed and turbulent kinetic energy at 2 m and 5 m above ground level for a westerly wind direction. Results show that all models predict the mean velocity reasonably well; however accurate prediction of the turbulent kinetic energy remains a challenge.

List of symbols

β	RNG k-ε model coefficient
ε	Turbulence dissipation rate, m^2/s^3
κ	von Karman constant
μ_t	Turbulent eddy viscosity, kg/m/s
η_0	RNG k-ε model coefficient
η	RNG k-ε model variable
ρ	Air density, kg/m^3
σ_k	k-ε model coefficient
σ_ε	k-ε model coefficient
$C_{1\varepsilon}$	k-ε model coefficient
$C_{2\varepsilon}$	k-ε model coefficient
C_μ	k-ε model coefficient
f_c	Coriolis factor,
G_k	Turbulence production rate, m^2/s^3
k	Turbulent kinetic energy, m^2/s^2
i,j,k	Co-ordinate subscripts
l_m	Mixing length, m
l_{max}	Mixing length limit, m
n_1	Distance from wall to first cell centre, m
P_ε	Production rate of ε, m^2/s^4
$\vec{U}_1$	Wind speed vector in first cell, m/s
$\vec{U}_g$	Geostrophic wind speed vector, m/s
u^*	Friction velocity, m/s
u_i	i^{th} component of mean velocity vector, m/s
x_i	i^{th} component of position vector, m
z_0	Aerodynamic roughness length, m

1. Introduction

Numerical wind flow modeling is a powerful tool for predicting quantities important to the wind energy industry, such as mean wind speed, turbulence intensity and inflow angle. However, such models invariably represent a simplified version of the full flow physics and the uncertainty associated with their predictions must be evaluated and, more importantly, minimized.

One of the best ways to achieve this is through validation against field measurement campaigns. This implies the installation of a set of well-equipped meteorological masts along main flow directions preferably fitted with high-frequency sonic anemometers to properly evaluate the statistical properties of turbulent flow.

Unfortunately, since the Askervein hill project in 1982-83 [1], no other detailed experiment meeting the above requirements had been carried out until the Bolund experiment [2,3], which took place over a three-month period in 2007-08. This experiment, organized by Risø DTU, consists of an extensive field measurement campaign of the flow over a 12 m-high small coastal island. The resulting dataset was the basis for the Bolund blind comparison [4] and is intended for use in the validation of wind flow models over complex terrain. In the blind comparison, the wind flow modeling

community was challenged to predict the speed-up factors and turbulent kinetic energy around the hill given only the inflow and topography. The compilation of the collective results provides a measure of the uncertainty for each type of approach and a general indication of the present state-of-the-art of wind flow modeling.

In this context, the present paper provides a summary of three CFD wind flow models that participated in the Bolund blind comparison and their respective predictions. The Bolund experiment is first described briefly in Section 2, including the layout of the meteorological masts as well as the types of sensors used. Section 3 describes in detail the main features of the RANS-based wind flow models developed by CENER (two models) and ÉTS (one model). The models are similar in many respects; most notably, they both employ two-equation turbulence closure. Furthermore, both ignore thermal effects, as prescribed in the blind comparison instructions. Their primary difference concerns the inclusion of the Coriolis force and the limitation (or not) of the turbulence length scale. The predictions of each model are presented in Section 4 where profiles of normalized mean velocity and turbulent kinetic energy are compared with measurements for a westerly wind. The results also include an analysis of the differences between the two models developed by CENER regarding the resolved turbulence length scale.

2. Bolund blind comparison

The Bolund experiment represents one of the most complete field datasets for the purposes of wind flow validation. The experiment was carried out by Risø DTU in 2007-08 over a 12m-high hill characterized by a complex topography and surrounded by water (see figure 1).

A layout of ten meteorological masts, M0 to M9, of 15-m height were installed along two lines (A and B), corresponding to inflow wind directions of 239° and 270°, respectively. Each mast was equipped at four heights (2, 5, 9 and 15 m above ground level (agl)) with cup and sonic anemometers. Additionally, LIDARs were located next to masts M2 and M9.

The dataset was filtered and averaged for four cases corresponding to wind directions of 239º, 255º, 270º, and 90º. Undisturbed conditions for flow cases 1 to 3 were derived from reference mast M0 located to the west of Bolund whereas the inflow for case 4 was determined by means of reference mast M9 located to the east.

The main results used to evaluate code performance are the mean wind speed and turbulent kinetic energy normalized by the corresponding undisturbed wind speed and square of the undisturbed wind speed at the reference mast, respectively. These values were extracted from the dataset for the different flow cases and measurement heights. Although wind speed and turbulent quantities were measured at 4 heights, only those at 2 m and 5 m agl are considered.

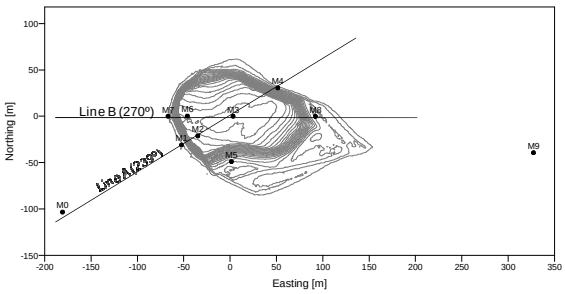

Figure 1. Bolund experiment

Topography and roughness definition files, as well as suggested inflow conditions, were provided to all participants in order to facilitate the comparison of results.

3. CFD wind flow models

Three different wind flow models are presented here; one of them has been developed at ÉTS and the other two at CENER. This section describes their main features and discusses some critical aspects of the simulations, such as mesh generation (domain extents, methodology and resolution), boundary conditions (especially the inflow and rough wall treatment), and finally the numerical methods (finite volume schemes).

3.1 CENER surface and atmospheric boundary layer models (CFDWind 1.0 and 2.0)

The non-linear CFD code CFDWind is based on the commercial software package FLUENT 12.0 [5], specifically adapted for the simulation of the mean wind components and turbulence intensity in the surface boundary layer (SBL) and atmospheric boundary layer (ABL). The SBL

corresponds (approximately) to the lowest 10% of the ABL which, in dimensional terms and depending on stability conditions and boundary layer depth, is on the order of 10s or 100s of metres. In both cases, air is considered an incompressible fluid and thermal effects are neglected.

CFDWind solves the Reynolds-Averaged Navier Stokes (RANS) equations (*i.e.* conservation of mass and momentum) as well as turbulence transport equations adapted to boundary layer flow. The model can be solved in SBL or ABL form:

- CFDWind 1.0 is based on Monin-Obukhov similarity theory for the SBL using the standard k-ε turbulence model with coefficients calibrated for atmospheric flows [6,7]. The model is described by the standard transport equations for k and ε in steady-state, three-dimensional form:

  Equation (1)

$$\frac{\partial}{\partial x_i}(\rho k u_i) = \frac{\partial}{\partial x_i}\left[\left(\frac{\mu_t}{\sigma_k}\right)\frac{\partial k}{\partial x_j}\right] + G_k - \rho\varepsilon$$

  Equation (2)

$$\frac{\partial}{\partial x_i}(\rho \varepsilon u_i) = \frac{\partial}{\partial x_j}\left[\left(\frac{\mu_t}{\sigma_\varepsilon}\right)\frac{\partial \varepsilon}{\partial x_j}\right] + C_{1\varepsilon}\frac{\varepsilon}{k}G_k - C_{2\varepsilon}\rho\frac{\varepsilon^2}{k}$$

  G_k is the turbulence production rate due to mean velocity gradients. The turbulent viscosity is computed as

$$\mu_t = \rho \cdot C_\mu \frac{k^2}{\varepsilon} \qquad (3)$$

  and model coefficients are calibrated to surface layer flow:

  C_μ=0.033; $C_{1\varepsilon}$=1.176; $C_{2\varepsilon}$=1.92; σ_k=1.0; σ_ε=1.3

  This model implicitly assumes that the mixing length is proportional to wall distance, increasing linearly with height agl as

$$l_m = \kappa z \qquad (4)$$

  where the von Karman constant is taken as ~0.41.

- CFDWind 2.0 is based on the limited-length-scale k-ε ABL model of Apsley and Castro (see [8]), which includes Coriolis and pressure gradient forces through geostrophic equilibrium conditions [9].

  As introduced by [10], limitation of mixing length growth is necessary in order to decrease turbulent mixing in the upper part of the boundary layer, which would otherwise lead to an ABL that is far too deep. This is achieved by modifying the production of ε (*i.e.* the $C_{1\varepsilon}$ term) in equation (2) as follows:

$$\left[C_{1\varepsilon} + (C_{2\varepsilon} - C_{1\varepsilon})\frac{l_m}{l_{\max}}\right]G_k\frac{\varepsilon}{k} \qquad (5)$$

  where the mixing length is calculated as

$$l_m = \frac{C_\mu^{3/4}k^{3/2}}{\varepsilon} \qquad (6)$$

  and l_{max} is estimated with

$$l_{\max} = 0.00027\frac{|\vec{U}_g|}{f_c} \qquad (7)$$

  $|U_g|$ is the modulus of the geostrophic wind and f_c accounts for Coriolis effects. For the Bolund location and estimated geostrophic wind, l_{max} is 25.2 m. This parameter is of particular importance as it diminishes the turbulent viscosity and consequently impacts momentum transport and the resolved wind speed distribution.

  An advantage of this model is that for large heights (as $l_m \rightarrow l_{max}$), the source terms in the ε equation cancel and ε (and consequently the mixing length) becomes constant and yet, near the wall (where $l_m << l_{max}$), the model remains consistent with the log-law in the surface layer as prescribed in CFDWind1.0 [9].

  For this version of the model, the k-ε coefficients are set according to [8]:

  C_μ=0.0256; $C_{1\varepsilon}$=1.13; $C_{2\varepsilon}$=1.9; σ_k=0.74; σ_ε=1.3

  Computational domain: The model is solved in a computational domain of 1260 m (E-W direction), 1170 m (N-S direction) and 300 m in the vertical direction for CFDWind 1.0. The domain is extended to a height of 1700 m for CFDWind 2.0. The domain is discretized with a structured grid, generated using the commercial

software ICEM CFD 11.0 Hexa, resulting in 3 million and 4.25 million hexahedral cells for CFDWind 1.0 and CFDWind 2.0, respectively. The near-wall cell height is 2.5 cm.

Boundary conditions for CFDWind 1.0: The inlet boundary conditions are defined by the vertical profiles of wind speed, turbulent kinetic energy and turbulence dissipation rate as specified by [11] for the SBL. The outlet boundary is defined as a pressure outlet and, for the top boundary, fixed values of wind speed and turbulent quantities are set in an effort to preserve constant shear stress. Symmetry conditions are imposed at the lateral boundaries.

Boundary conditions for CFDWind 2.0: The inlet boundary conditions are defined by the vertical profiles of wind speed components, turbulent kinetic energy and turbulence dissipation rate from a preceding 1D simulation of a steady-state turbulent atmospheric boundary layer. The outlet boundary is defined as a pressure outlet and a symmetry condition is specified at the top. Periodic conditions are imposed at the lateral boundaries.

The ground is simulated as a wall for both models, through adaptation of the standard wall functions, by establishing a link between the turbulent law-of-the-wall modified for mechanical roughness and the surface boundary layer log-law based on the roughness length. The method proposed by [12] for FLUENT 12.0 is used.

Numerical method: After the grid is generated, a control-volume technique is used to convert the governing differential equations into algebraic equations that can be solved numerically. A second-order upwind scheme based on a multi-linear reconstruction approach is used for all dependent variables [13].

3.2 ÉTS surface boundary layer model

The ÉTS model solves the RANS equations using the RNG k-ε model for closure [14]. The RNG model consists of turbulence transport equations identical to (1,2) except for an additional source term in the ε equation given by

$$P_\varepsilon = \frac{C_\mu \eta^3 (1-\eta/\eta_0)}{1+\beta\eta^3} \cdot \frac{\varepsilon^2}{k} \qquad (8)$$

where η is related to the magnitude of the mean strain rate tensor. Use of the RNG model has been previously reported to improve flow predictions where recirculation is present (see, for example, [15]) and is adapted here for surface layer flow by adjusting the turbulence coefficients as suggested in [16]. The von Karman constant is taken equal to 0.40 and Coriolis effects are neglected.

Computational domain: The overall domain length, width and height are 990 m, 650 m, and 120 m, respectively. To generate the grid, a Cartesian surface mesh aligned with the inflow is interpolated from the supplied topography file and then extrapolated vertically to fill the domain. A geometric expansion is used to ensure high cell density in regions of large gradients; near-wall cell heights are everywhere less than 10 cm. The mesh contains a total of roughly 8 million cells.

Boundary conditions: Constant flow properties for wind speed and turbulence are specified at the upper boundary and a symmetry condition is used for the lateral boundaries. The inflow is defined as suggested by Risø DTU and the outflow assumed to be fully-developed. The most sensitive boundary condition is that of the ground and the treatment of surface roughness. Here, z_0-based wall functions are used to set the values of k and ε in the near-wall cell based on the local wall friction velocity

$$u^* = \frac{|\vec{U}_1|}{\ln(n_1/z_0)} \qquad (9)$$

A retarding shear stress is specified for the momentum equations also based on this quantity.

Numerical method: OpenFOAM [17] is used to solve the system of equations using the SIMPLE method to handle pressure-velocity coupling. Diffusion terms are discretized using central-differencing while convection terms are discretized using first-order upwind differencing.

4. RESULTS

The axial evolution along line B of speed-up factor, normalized turbulent kinetic energy, and turbulence length scale are presented in figures

2 through 6 for an inflow wind direction of 270º. For the length scale analysis, only the results of CFDWind 1.0 and CFDWind 2.0 are presented for the purposes of evaluating the effect of limiting the length scale on the wind speed and turbulence predictions. Sensors at all levels correspond to sonic anemometers except at reference masts M0 and M9 at 2m agl, where only cup anemometers were installed.

4.1 Speed-up factors

Figures 2 and 3 present the axial evolution of speed-up factor along line B at 2 m and 5 m agl for an inflow wind direction of 270º. The predicted and measured mean wind speeds at the reference meteorological mast, M0, have been used to normalize the results. In order to quantify the inherent variability of wind speed, data plots include bars which represent ± one standard deviation.

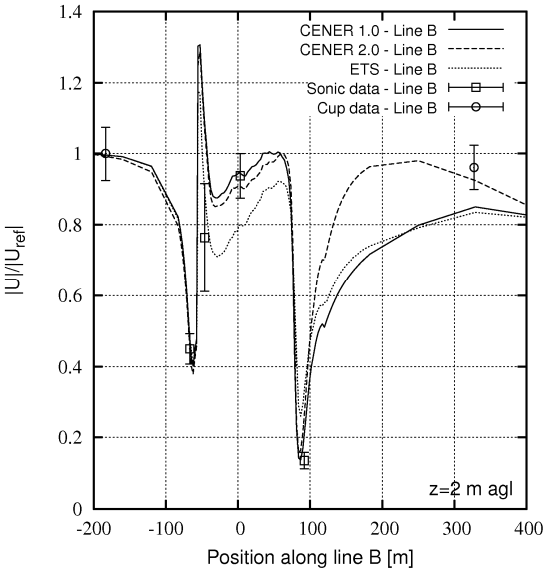

Figure 2. Speed-up factors at 2 m agl along line B for a wind flow direction of 270 degrees

As can be observed, both models are fairly good at predicting the speed-up factor, even in the areas of possible flow separation at the top of the hill and downstream in its wake. Although some of the discrepancies between the model predictions may be due to differing grids and slightly different boundary conditions, the main discrepancies are expected to stem from the methods by which the turbulent length scale is estimated (*i.e.* the ε equation). This can be seen downstream of the first escarpment where, although the predicted turbulent kinetic energy of all models is similar, use of the RNG turbulence model appears to lead to a slower recovery of the flow with respect to standard k-ε and the Apsley and Castro length-limited version.

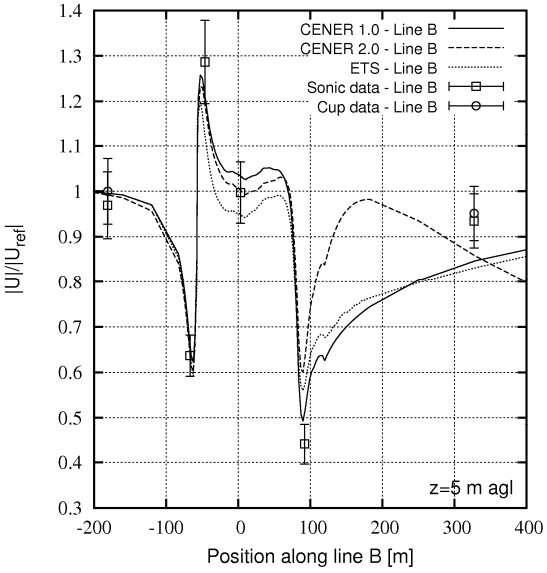

Figure 3. Speed-up factors at 5 m agl along line B for a wind flow direction of 270 degrees

In the wake region of the hill, the flow recovery predicted by CFDWind 2.0 is somewhat unexpected and also explained by the modified ε equation specific to the Apsley and Castro approach. This behavior is due to the limiting of the turbulent length scale and will be discussed further in Section 3.3.

A mean absolute error (*mae*) of predicted speed-up factor with respect to the experimental data can be quantified as

$$mae = \frac{\Sigma \left| F_{predicted} - F_{measured} \right|}{N} \qquad (10)$$

where:

$F_{predicted}$ = predicted speed-up factor

$F_{measured}$ = measured speed-up factor

N = number of points

Table 1 presents the mean absolute errors at 2 m and 5 m agl in addition to maximum and minimum values. As might be expected, the errors are higher at 2 m where discretization error may be important and predictions are likely most sensitive to turbulence modeling and the prescribed wall boundary conditions.

Z (m)		CFDWind1	CFDWind2	ETS
2m	ave	0.087	0.109	0.126
	min	0.001	0.001	0.034
	max	0.313	0.297	0.196
5m	ave	0.051	0.058	0.100
	min	0.021	0.001	0.003
	max	0.081	0.184	0.186

Table 1. Mean, maximum and minimum absolute errors of speed up factors at 2 m and 5 m agl

4.2 Normalized turbulent kinetic energy

Figures 4 and 5 present the axial evolution of the normalized turbulent kinetic energy at 2 m and 5 m agl for the same inflow wind direction. The square of the undisturbed velocity at the reference meteorological mast, M0, has been used to normalize the results.

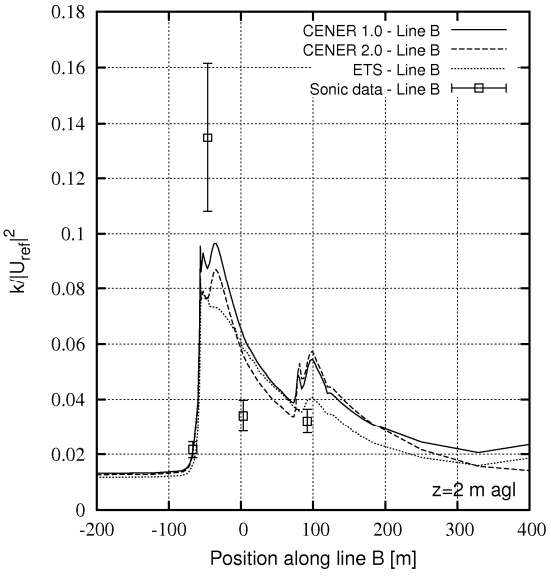

Figure 4. Normalized k at 2 m agl along line B for a wind flow direction of 270 degrees

In general, the three models over-predict the magnitude of k, the only exception being at 2 m agl just downstream of the cliff edge where the observed turbulence level is quite high. Contrary to model predictions, this peak is not observed at 5 m. The tendency of k-ε models to over-estimate the turbulent viscosity in zones of high curvature is noticeable at 5 m. The models predict two zones of elevated turbulence whereas the data seems to indicate just one zone on the lee side of the hill.

The mean absolute error of predicted k can also be quantified with respect to the experimental data and is shown in table 2, using the same definition as equation (10). Again, it is seen that the level of error is higher at 2 m than at 5 m. The overall error of each model is roughly the same.

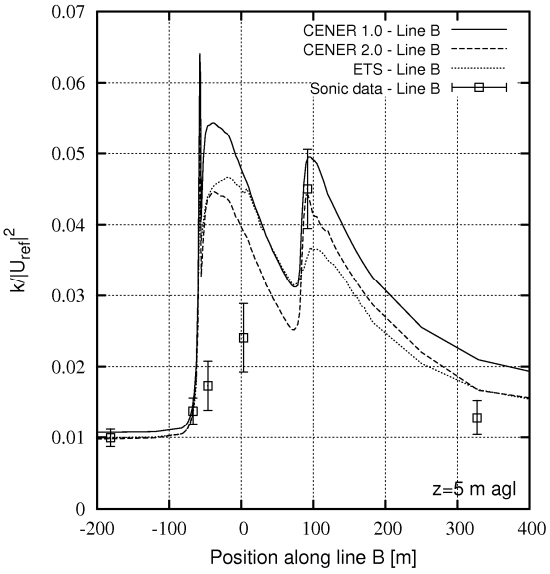

Figure 5. Normalized k at 5 m agl along line B for a wind flow direction of 270 degrees.

Z (m)		CFDWind1	CFDWind2	ETS
2m	ave	0.024	0.026	0.024
	min	0.001	0.001	0.006
	max	0.048	0.059	0.060
5m	ave	0.011	0.008	0.010
	min	0.001	0.000	0.000
	max	0.036	0.026	0.027

Table 2 Mean, maximum and minimum absolute errors of normalized k at 2m and 5m agl

4.3 Turbulence length scale

From equation (6), the turbulence length scale can equivalently be calculated as

$$l_m = \frac{\mu_t}{C_\mu^{0.25} k^{0.5}} \qquad (11)$$

The influence of the length-scale-limiting Apsley and Castro ε equation on the resolved mixing length can be seen in figure 6 which presents the variation of l_m along line B at 5 m agl for the two versions of CFDWind.

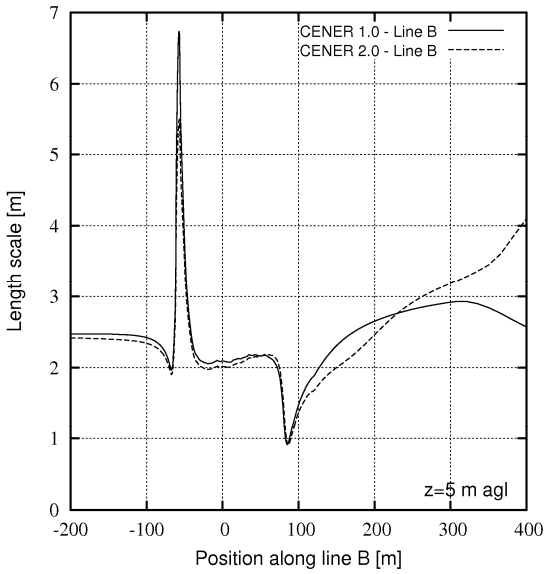

Figure 6. Turbulence length scale at 5 m agl along line B for a wind flow direction of 270 degrees (CFDWind 1.0 and 2.0)

The profiles are everywhere similar except at the leading edge of the escarpment, where the speed-up is the highest, and in the wake of the hill. Both CFDWind 1.0 and 2.0 overestimate k in stagnation areas (like at the escarpment) which is a well-known problem of k-ε models in bluff body aerodynamics. The effect seems to be more pronounced for CFDWind 1.0.

In the wake of the hill, CFDWind 2.0 progressively increases the mixing length due to a rapid reduction of ε near the wall which, as a consequence, increases the turbulent viscosity and produces a faster recovery of the wind speed, as observed in figures 2 and 3. The subsequent decrease in wind speed is currently being investigated.

4. Conclusions

Participation of the presented flow models (and others) in the Bolund blind comparison has demonstrated that RANS modeling with two-equation k-ε closure, properly modified for the simulation of the surface or atmospheric boundary layer, can provide reasonably accurate flow predictions over complex terrain. Here, the mean absolute error in normalized velocity for all models was on the order of 10^{-1}, while for normalized turbulent kinetic energy was 10^{-2}. Given the nature of a blind test, these errors should be regarded as upper limits as practical application of such models generally involves the calibration of boundary conditions and model coefficients to site conditions. These limits will surely decrease in the future with improvements in turbulence modeling.

Full ABL models like the one implemented in CFDWind 2.0 impose a limit on the turbulence length scale which should improve wind speed predictions outside the surface layer. This effect is clearly desirable for multi-megawatt wind turbine heights, but the consequences of such an approach for the near-ground flow over complex terrain, especially in areas of recirculation, require further investigation.

References

[1] Taylor, P. and Teunissen, H., “The Askervein Hill project: Overview and background data”, *Boundary-Layer Meteorology*, 1987, 39, 15-39

[2] Bechmann A., *et al.* “The Bolund experiment: A validation dataset”, Risø DTU, http://bolund.risoe.dk

[3] Bechmann A., Berg J., Courtney M., *et al.*, “The Bolund experiment: Overview and background”, Risø-R-1658(EN), 2009

[4] Bechmann A., *et al.*, “The Bolund experiment: Blind comparison of flow models”, Risø DTU, http://bolund.risoe.dk

[5] Fluent Inc., “Fluent 12.0 User's Guide”, Fluent Inc., October 2009

[6] Alinot, C. and Masson, C., "k–ε model for the atmospheric boundary layer under various thermal stratifications", *Journal of Solar Energy Engineering - Transactions of the ASME*, 2005, 127, 438-443

[7] Sanz Rodrigo J., Cabezón D., Martí I., Patilla P., van Beeck J., "Numerical CFD modelling of non-neutral atmospheric boundary layers for offshore wind resource assessment based on Monin-Obukhov theory", in scientific proceedings of EWEC-08, Brussels (Belgium), April 2008

[8] Apsley D.D. and Castro I.P., "A limited-length-scale k–ε model for the neutral and stably-stratified atmospheric boundary layer", *Boundary-Layer Meteorology*, 1997, 83, 75-78

[9] Sanz Rodrigo J., Cabezón D., Lozano S., Martí I., "Parameterization of the atmospheric boundary layer for offshore wind resource assessment with a limited-length-scale k-ε model", in scientific proceedings of EWEC-09, Marseille (France), March 2009

[10] Detering H.W and Etling D., "Application of the k–ε turbulence model to the atmospheric boundary layer", *Boundary-Layer Meteorology*, 1985, 33, 113-133

[11] Richards, P.J. and Hoxey, R., "Appropriate boundary conditions for computational wind engineering models using the k–ε turbulence model", *J. Wind Eng. Ind. Aerodyn.*, 1993, 46-47, 145–153

[12] Blocken B., Stathopoulos T., Carmeliet, J., "CFD simulation of the atmospheric boundary layer: Wall function problems", *Atmospheric Environment*, 2007, 41, 238-252

[13] Barth T.J. and Jespersen D., "The design and application of upwind schemes on unstructured meshes", AIAA paper 89-0366, 1989

[14] Yakhot, V. and Orszag, S.A., "Renormalization Group Analysis of Turbulence. I. Basic Theory", *J. Sci. Comput.*, 1986, 1, 3-51

[15] Maurizi, A. "Numerical simulation of turbulent flows over 2-D valleys using three versions of the k–ε closure model", *J. Wind Eng. Ind. Aerodyn.*, 2000, 85, 59–73

[16] El Kasmi, A. and Masson, C., "Turbulence modeling of atmospheric boundary layer flow over complex terrain: A comparison of models at wind tunnel and full scale", *Wind Energy*, in print

[17] OpenCFD, "OpenFOAM: The Open Source CFD Toolbox – Programmer's Guide v1.6", 2009